MINIREVIEW

Measuring Rotations of a Few Cross-Bridges in Skeletal Muscle

JULIAN BOREJDO,[1] JOHN TALENT, AND IRINA AKOPOVA

Department of Molecular Biology and Immunology, the University of North Texas Health Sciences Center, Fort Worth, Texas 76107

The ability to measure properties of a single cross-bridge in working muscle is important because it avoids averaging the signal from a large number of molecules and because it probes cross-bridges in their native crowded environment. Because the concentration of myosin in muscle is large, observing the kinetics of a single myosin molecule requires that the signal be collected from small volumes. The introduction of small observational volumes defined by diffraction-limited laser beams and confocal detection has made it possible to limit the observational volume to a femtoliter (10^{-15} liter). By restraining labeling to 1 fluorophore per 100 myosin molecules, we were able to follow the kinetics of approximately 400 cross-bridges. To reduce this number further, we used two-photon (2P) microscopy. The focal plane in which the laser power density was high enough to produce 2P absorption was thinner than in confocal microscopy. Using 2P microscopy, we were able to observe approximately 200 cross-bridges during contraction. The novel method of confocal total internal reflection (CTIR) provides a method to reduce the observational volume even further, to approximately 1 attoliter (10^{-18} liter), and to measure fluorescence with a high signal-to-noise (S/N) ratio. In this method, the observational volume is made shallow by illuminating the sample with an evanescent field produced by total internal reflection (TIR) of the incident laser beam. To guarantee the small lateral dimensions of the observational volume, a confocal aperture is inserted in the conjugate-image plane of the objective. With a 3.5-μm confocal aperture, we achieved a volume of 1.5 attoliter. Association-dissociation of the myosin head was probed with rhodamine attached at cys707 of the heavy chain of myosin. Signal was contributed by one to five fluorescent myosin molecules. Fluorescence decayed in a series of discrete steps, corresponding to bleaching of individual molecules of rhodamine. The S/N ratio was sufficiently large to make statistically significant comparisons from rigor and contracting myofibrils. Exp Biol Med 231:28–38, 2006

Key words: muscle contraction; confocal microscope; 2P microscope; TIR microscope

Muscle contraction results from interactions of the myosin subfragment-1 (S1) with actin. S1 consists of the N-terminal catalytic domain and the C-terminal regulatory domain. The atomic structure of S1 suggests that the regulatory domain acts as a "lever-arm" that translates small conformational changes occurring in the catalytic domain after ATP hydrolysis to a large linear motion of the thick filaments (1). This idea is consistent with early experiments showing rotary motion of the regulatory domain (2, 3) and with recent experiments showing correlation between the length of the regulatory domain and the velocity of *in vitro* motion (4, 5). S1 crystal structure showed directly that the regulatory domain assumed a different orientation in the absence (1) and in the presence (6) of nucleotides. It is thought that the swing of the regulatory domain is caused by a specific event during the ATPase cycle of a cross-bridge. Thus, measuring the orientations of cross-bridges in muscle is a key to understanding the molecular mechanism of muscle contraction.

Spectroscopic methods offer a convenient way to address this problem (7). In particular, fluorescence polarization or anisotropy (8–21) have been exploited to take advantage of their ability to measure orientation of cross-bridges in different physiologic states.

However, all measurements to date have been performed using a large population of cross-bridges. In

Supported by grants R21CA9732 and R01 AR048622 from the National Institutes of Health to J.B.

[1] To whom correspondence should be addressed at: Department of Molecular Biology and Immunology, University of North Texas, Fort Worth, TX 76107. E-mail: jborejdo@hsc.unt.edu

1535-3702/06/2311-0028$15.00

such experiments, the anisotropy is averaged over an entire assembly of observed cross-bridges. However, each cross-bridge has different kinetics, depending on its position relative to the actin-binding site (22). Serious consequences of this fact are illustrated in Figure 1. If a single cross-bridge were observed, the anisotropy of the lever-arm would be expected to change in four steps that correspond to the cross-bridge release from actin, the free rotation, the weak binding, and the transition to a strongly bound state (power stroke) (Fig. 1A). However, if the number of observed cross-bridges is greater than one, these steps become obscured or their kinetics becomes altered. Although the number of observed cross-bridges does not matter for measurements of dissociation (because all of the cross-bridges dissociate from actin at the same time because of a rapid release of ATP from caged precursor and because of the rapidity of the cross-bridge dissociation), the number matters for measurements of cross-bridge rebinding and of the power stroke. This is because cross-bridges rebind to actin at different times. The amount of time that a cross-bridge remains free depends on its position relative to the actin target site (22, 23). If the observed population consists of 50 cross-bridges, the four steps and their timings are approximately conserved (Fig. 1B), but if it consists of as few as 300 (Fig. 1C) or 1000 (Fig. 1D) cross-bridges, the critical steps are lost, and the kinetics are altered. Another complication of detecting motion of a large assembly of myosin heads is that anisotropy is measured from detached and weakly bound cross-bridges that do not contribute to force generation. They are disordered (24, 25) and their number is substantial (70%–80% of the total number of cross-bridges; refs. 26, 27).

Ideally, therefore, the anisotropy should be measured from a single molecule. This was recognized previously, and a number of elegant experiments has been performed on isolated myosin molecules *in vitro* (28–31). A single molecule was made fluorescent (by tagging the myosin light chain with rhodamine) and imaged by total internal reflection (TIR). Polarization of the fluorescence of the tag was measured in real time with millisecond time resolution. Data from smooth muscle provided direct evidence that the myosin light chain (regulatory) domain adopted at least two orientation states during the cyclic interaction of myosin with actin (30). In myosin V, it was possible to perform three-dimensional measurements of the structural dynamics of the light chain domain (28–31). Single fluorescent calmodulin light chains, which served as indicators of motion of the myosin light-chain domain, tilted back and forth between two well-defined angles as the myosin molecule processively translocated along the actin. These experiments represented a technical breakthrough, and were an impressive demonstration that myosin lever-arm rotations occurred during the translocation of the myosin molecules along the actin filaments.

However, these measurements were performed on isolated myosin molecules. It is likely that cross-bridges in functioning muscle behave differently than purified myosin in solution. The mechanism that is most likely responsible for the different properties of myosin in solution compared with myosin in muscle fibers is molecular crowding. The intact muscle fiber is a remarkably crowded environment, with approximately 23% of the muscle weight contributed by protein. Crowding influences protein solubility and conformation in solution (32, 33). In the environment of the muscle fiber, crowding may impose constraints affecting both the structure and function of myosin. The effect of crowding on myosin can be demonstrated in solution by addition of large co-solvent molecules, for instance, polyethylene glycol (PEG). PEG is excluded from a volume adjacent to the surface of the molecule, that is, smaller water molecules preferentially contact the protein surface and induce hydration of the protein (34). Preferential hydration leads to aggregation, because proteins change conformation to reduce their exposure to water, as shown by Minton (35, 36) and Timasheff (33, 37). Highsmith *et al.* (38) found that the reversible PEG-induced S1 aggregation is accompanied by the loss of its Mg-mediated ATPase activity. This loss was shown by Muhlrad *et al.* to be caused by the inhibition of the myosin lever-arm motion (39). Molecular crowding may provide a rationale for the two different myosin cross-bridge orientations that are observed in rigor complexes formed at different degrees of saturation of actin filaments with S1 (40, 41).

The lack of a crowded environment may be responsible for the fact that movement in solution may be generated differently than in muscle. Sutoh *et al.* (42) showed that, *in vitro*, Dictyostelium S1 devoid of the regulatory domain was able to drive the sliding movement of actin filaments. Yanagida *et al.* (43) showed that S1, attached to a glass surface through a flexible random chain, moved actin as fast as intact myosin. Recently, Yanagida *et al.* showed that myosin devoid of most of the light chain–binding domain gave the same displacement as intact myosin (44). Moreover, some data suggest that, *in vitro*, there is only a loose connection between mechanical and enzymatic events. Thus, the sliding distance in an *in vitro* assay (near zero load) was reported to be greater than 100 nm during one ATP hydrolysis cycle (45). Force generation did not coincide with the release of ADP and, instead, *in vitro*, the myosin head was shown to produce force several hundreds of milliseconds after bound nucleotide was released (29). In relaxed scallop muscle, the rotation of the regulatory domain was not coupled to a specific step in the ATPase cycle (46).

We, therefore, think that rotation of the myosin lever arm of a single cross-bridge should be measured in working muscle. This is not a simple task, because myosin in muscle is highly concentrated (47). To observe a single molecule in muscle, it is necessary to collect data from extremely small volumes. The observational volume of conventional wide-field microscopes is excessively large ($\sim 10^{-9}$ liter). There are approximately 100 billion myosin molecules in this

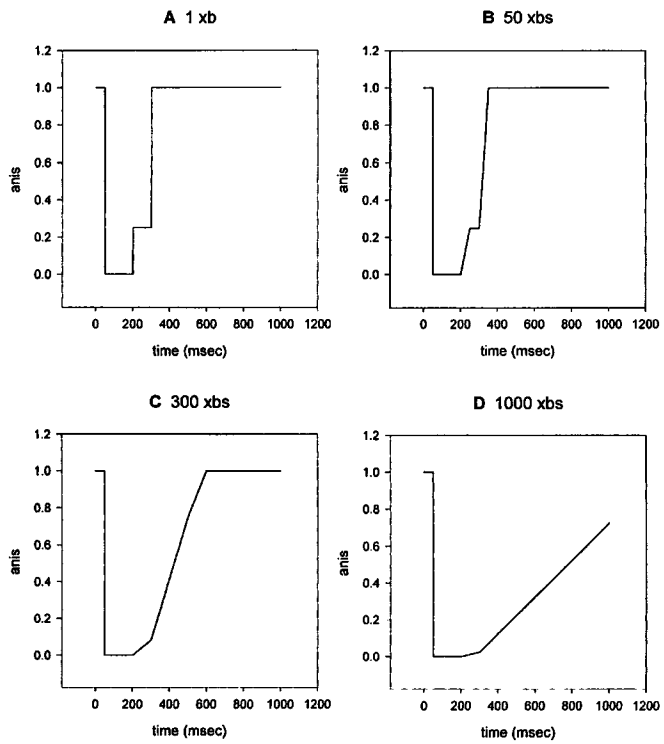

Figure 1. Effect of increasing the number of observed cross-bridges on anisotropy. When a single cross-bridge is observed, the anisotropy changes in a step-wise manner (A). When the number observed is sufficiently small, the steps are preserved (B). However, when a large number is observed, the anisotropy changes smoothly (C and D). It is assumed that all cross-bridges dissociate from actin at the same time (at time 0), but remain unbound depending on their position relative to the actin target site. It is assumed here for simplicity that this time differs by 1 msec for each cross-bridge. (Reprinted with permission from Ref. 52).

volume. The introduction of small observational volumes defined by diffraction-limited laser beams and confocal detection has made it possible to limit the observational volume to a femtoliter (10^{-15} liter) and to eliminate much of the background noise (48). Although the observational volume of a confocal microscope is still relatively large, we have used it to measure anisotropy of small numbers of cross-bridges in muscle (49–51). By restraining the labeling to 1 fluorophore for 100 myosin molecules, the number of observed cross-bridges was approximately 400 (50). Table 1 summarizes this method.

To reduce the number further, we used two-photon (2P) microscopy (52). In conventional confocal (1P) microscopy, the thickness of the observational volume is defined by the diameter of the confocal aperture. In previous experiments, the aperture was 35 μm.[1] Thus, the depth-of-focus was approximately 3 μm, the volume was approximately 0.3 μm^3, and the number of observed cross-bridges was approximately 400. In 2P microscopy, which is now possible because of the wide availability of ultra-short, pulsed, near-infrared (IR) lasers, the signal originates only from the focal plane in which the laser power density is high enough to produce 2P absorption (53). In our experiments, this plane was one-half as thin as in confocal microscope, allowing us to observe approximately 200 cross-bridges. Although the number of observed cross-bridges was reduced by one-half, the signal-to-noise (S/N) ratio was unchanged. This was because the 2P photobleaching was reduced and because the absolute values of the 2P anisotropy were larger. Out-of-focus photobleaching is reduced in 2P because out-of-focus planes are illuminated by less-damaging IR light. Surprisingly, in the case of muscle exchanged with myosin light chains labeled with rhodamine, photobleaching in the plane of focus was also reduced. The anisotropy was larger because absorption to emission ratio of two photons depends on the fourth power (not the second power like 1P absorption) of the cosine of the angle between the dye dipole and the direction of polarization of the excitation light. Thus, four important advantages of 2P microscopy over confocal microscopy were exploited. First, the observed volume, and, hence, the number of observed cross-bridges was smaller; second, photobleaching was less destructive; third, the change in signal was larger; and fourth, the signal was observed through a side port, therefore, fluorescent light did not enter the microscope and, thus, was not attenuated by the microscope optics. Using 2P microscopy, we were able to observe approximately 200 cross-bridges during contraction and to resolve more details of the cross-bridge cycle; specifically, the outset of the power stroke (52). Table 1 summarizes these methods.

The experiments illustrating the use of confocal and 2P are briefly described next. Myosin was labeled by incorporating recombinant regulatory light chain (RLC) labeled with rhodamine, as described in (54). After a 0.5-hr incubation at 30°C, it was observed that 25% of the myosin molecules had undergone exchange, that there was no unspecifically bound RLC, and that exchanged muscle developed normal isometric tension. In a typical experiment, 2% of the myosin molecules in the fibers were labeled (incubation for 15 mins, at room temperature, with 0.28 mg/ml RLC). We first describe measurements obtained using a confocal microscope. Actin labeled with fluorescein isothiocyanate (FITC)-phalloidin (55) was used as a control. Fibers were observed through either fluorescein (Fig. 2A) or rhodamine (Fig. 2B) filters. In the images, the objective focuses visible laser light onto the A-band (white spot). The width and depth of the spot are approximately equal to the diffraction limit (~0.3 μm). The height is defined by the diameter of the confocal aperture. Unless otherwise stated, the height is approximately 3 μm (Fig. 2D, right panel). The approximately 0.3 μm^3 volume observed contained approximately 400 labeled cross-

[1]It could not be further decreased, because closing it decreased the S/N ratio to the extent that measurements became impossible.

Table 1. The Number of Observed Molecules in Wide-Field, Confocal, and 2P Microscopy

Method	Experimental volume (liter)	Approx. no. of cross-bridges in the volume	Degree of labeling (%)	Approx. no. of observed (fluorescent) cross-bridges	Reference
Wide field	10^{-9}	10^{11}	63	6×10^{10}	(54)
Confocal	0.3×10^{-15}	2×10^{4}	2	400	(51)
2P	0.2×10^{-15}	10^{4}	2	200	(24)

bridges and approximately 1000 labeled actin monomers. The microscope was operated in "spot" mode (i.e., a single spot, located exactly in the center of the field of view, was illuminated). The beam was not scanned. The laser power incident on image plane was typically a few milliwatts. This power was concentrated at one spot on a sample for the duration of the entire experiment (6.5 secs), leading to considerable photobleaching. For example, if the power is 2 mW and the spot size is 0.5×0.5 μm, the power density is very large, at 0.8×10^5 J/(cm^2·sec). To minimize this effect, the laser light was attenuated 1000 times (the power incident on the fiber = 2.3 μW; dark gray in Fig. 2D). The same volume was illuminated with the UV light to produce ATP (dashed line). The details of the experimental arrangement are given elsewhere (50). A typical result (Fig. 3A) is discussed next.

In the confocal experiments described in the preceding paragraph, the thickness of the observational volume was defined by the diameter of the confocal aperture. At an aperture of 35 μm, the number of observed cross-bridges was approximately 400. Use of the 2P technique allowed observation of approximately 200 cross-bridges with an S/N ratio as good as in the ordinary confocal experiment. The experimental setup used in 2P experiments was similar to that used in ordinary confocal microscopy, except that the muscle was illuminated by femtosecond pulses from an IR laser (Mira, Coherent Inc., Santa Clara, CA) pumped by 6.5 W of 532-nm light from a Verdi Solid State laser (Coherent) (52). The IR laser beam was expanded by the beam expander, attenuated by neutral density filters, and passed to the x-y scanner, which projected the scanned beam onto the objective. The IR power impinging on the muscle was approximately 65 mW. Fluorescent light was collected by the objective and projected to a side port of a microscope. The rotational motions of cross-bridges were synchronized by rapid (10 msecs) photogeneration of ATP. During the 10 msecs, all caged ATP is converted to ATP (56). Because the root-mean-square velocity of diffusion of ATP, determined by its diffusion coefficient (3.7×10^{-6} cm^2/sec; ref. 57), is approximately 1 μm/msec, ATP diffuses away from the experimental volume in approximately 300 μsecs. Therefore, after 300 μsecs, there is practically no free nucleotide left in the experimental volume. Change of anisotropy after the pulse reflects the rotation caused by the turnover of a single molecule of ATP. In single-turnover experiments, cross-bridges rotate despite the fact that contraction is isometric. This is because after generation of ATP, rigor tension is released and the rotation of the cross-bridges is unopposed by series elasticity. Figure 3A compares 1P (top trace) and 2P (bottom trace) anisotropy changes of myosin after a pulse of UV light is applied (at arrow). After ATP is photogenerated, the anisotropy changes rapidly, indicating release of cross-bridges from thin filaments. The rate of this change was too rapid to be measured. After the rapid change, the anisotropy signal recovered slowly. The rate of this recovery was 1.57 sec^{-1} and 0.72 sec^{-1} for the 1P and 2P experiments, respectively. The 1P rate is in good agreement with previous results (50). We think that the rapid decrease represents dissociation of S1 from actin (18, 50) and that the slow recovery represents rebinding of the cross-bridges to thin filaments. The fact that the rate of slow recovery of anisotropy depended on the ATP concentration in a second-order fashion (18, 50) supports this conclusion. The rapid change and slow recovery are prolonged in our experiments because cross-bridges execute only a single-turnover event. After photocreation, ATP diffuses away from the experimental volume. In a single-turnover experiment, the cross-bridge detaches and reattaches only once, that is, after reattaching, the probability of detachment becomes 0. A cross-bridge that has finished the turnover cycle acts as a load for cross-bridges that have not completed the cycle. This load slows the contraction and slows the rate of anisotropy change. We estimated the change in kinetics of displacement by the Monte-Carlo method (as in Refs. 58 and 59). We constructed a stochastic model of muscle in which each cross-bridge had an associated probability of attachment and detachment that depended on its x-value (the position, x, being that of a cross-bridge–carrying ATP relative to the actin-binding site). These probabilities depend on the rates of cross-bridge attachment and detachment, $f(x)$ and $g(x)$ (23), as modified by Hill (60). Model calculations show that ATP diffusion slows the dissociation by a factor of approximately 15 and recovery by a factor of 2.7 (50, 51), suggesting that the steady-state rate of rebinding is 4.2 sec^{-1} (for 1P experiments). Similar results were obtained when essential light chain was used instead of RLC (52), and when human cardiac RLC containing a single cysteine at position 36 labeled with 5′-iodoacetamido-tetramethyl-rhodamine (IATR) was used (not shown; gift from Dr. D. Szczesna, University of Miami, Miami, FL).

Confocal and 2P microscopy offer no hope of further

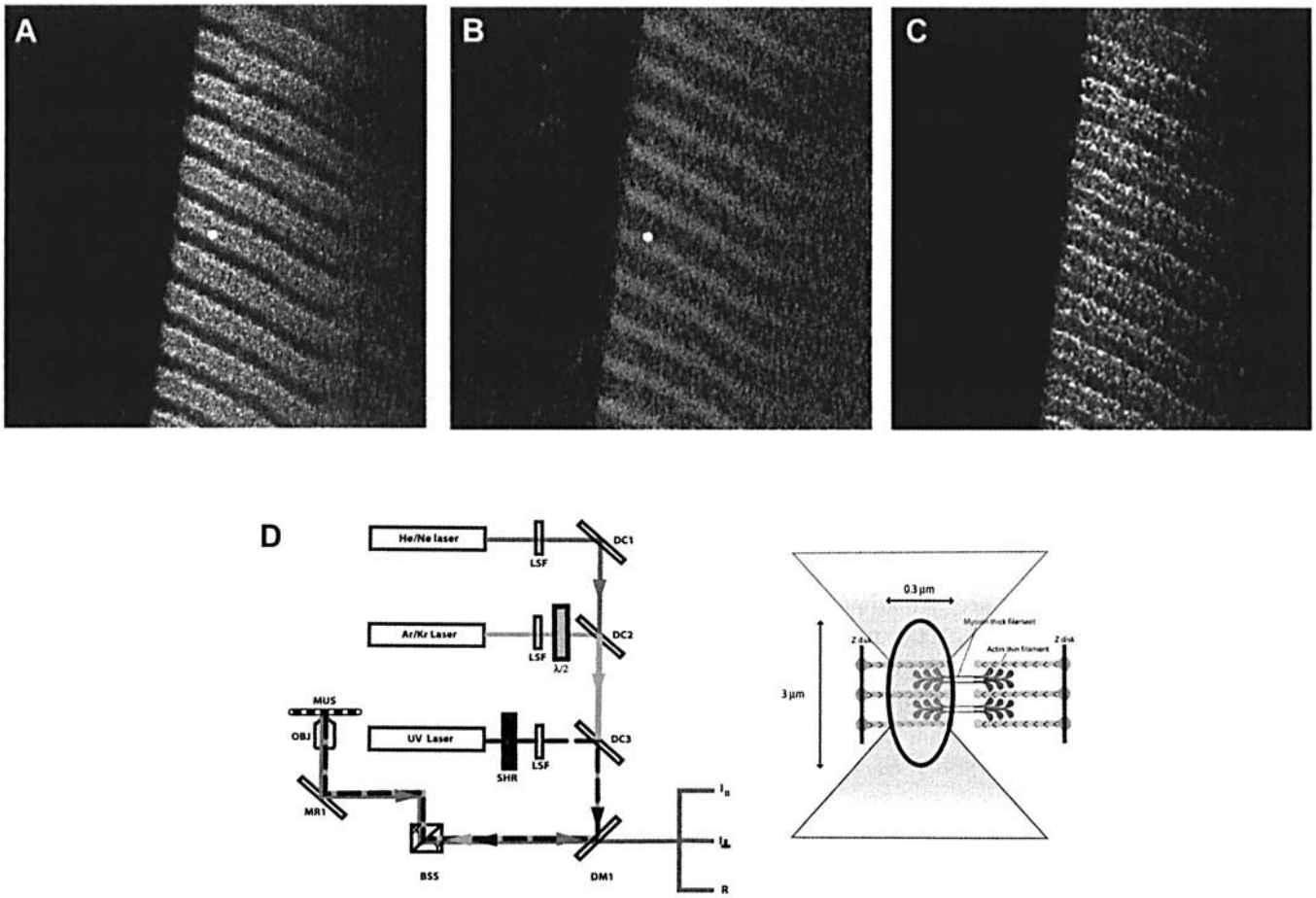

Figure 2. Labeling actin with FITC-phalloidin (left) and myosin with rhodamine-labeled RLC (middle) in the same muscle fiber results in staining of I- and A-bands. (A) Muscle was labeled with 0.3 μ*M* FITC-phalloidin for 0.5 hr and viewed through a band-pass ($515 < \lambda < 565$ nm) filter. Only the I-bands, containing fluorescent actin, are visible. The white spot indicates the size of the laser beam. (B) The same fiber was exchanged with rhodamine-labeled RLC and viewed through a long-pass ($\lambda > 590$ nm) filter. Only the A-bands, containing fluorescent myosin, are visible. The white spot indicates the size of the laser beam. (C) Composite of A and B. Sarcomere length = 2.65 μm. (D) Method of measuring anisotropy of fluorescence. (Left panel) 633-, 568-, or 488-nm light is projected onto muscle (MUS) through the objective (OBJ). The objective also collects fluorescent light and projects it onto photomultipliers that record perpendicular ($I_\perp$) and parallel ($I_\parallel$) components of polarized fluorescence. Mirrors of the beam scanner (BSS) are kept fixed at the $x = 0$, $y = 0$ position. (Right panel) Schematic view of the *z*-section of the focused laser spot shown in (A) and (B). (Reprinted with permission from Ref. 51).

decreasing the number of observable cross-bridges. In the case of confocal detection, the diameter of the confocal aperture, which determines the observational volume, cannot be decreased further without decreasing the S/N ratio below an acceptable level (50). In 2P experiments, the observational volume cannot be controlled at all. The only way to decrease the number of observable cross-bridges is to decrease the extent of labeling, but reducing the labeling to less than 2% is not reproducible and decreases the S/N ratio below a tolerable level. Therefore, a new method is required! The method described here, a combination of TIR and confocal microscopy (referred to as confocal TIR [CTIR]) offers hope of decreasing the number of observable cross-bridges.

CTIR defines an observational volume on the order of attoliters (10^{-18} liter). Such miniscule volumes have recently been obtained by other researchers by using zero-mode waveguides, which consist of small apertures in a metal film deposited on a coverslip (61). Such apertures act as sources of evanescent waves, therefore, the volume defined by each aperture is limited in the *z*-direction by the depth of the evanescent wave (~100 nm) and in the *x*- and *y*-directions by the size of the aperture. For example, if the aperture is 100 nm, the observational volume is approximately equal to an attoliter. However, manufacture of the film with small apertures is complex and expensive. Another way to decrease volume is to use near-field scanning optical microscopy (NSOM), in which an evanescent wave is produced by passing light through a narrow (50- to 100-nm) aperture (62–64). We have invested considerable effort and resources on this approach. In collaboration with Dr. A. Lewis at the Hebrew University of Jerusalem, Jerusalem, Israel, we were able to visualize 60 molecules by this method. However, the method requires that the NSOM

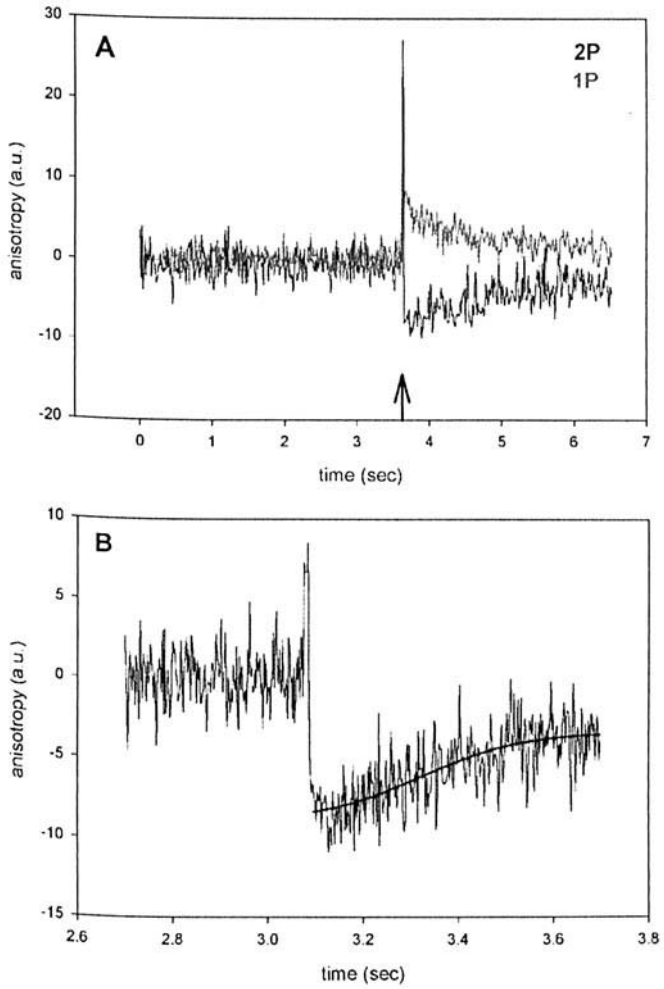

Figure 3. Anisotropy of myosin cross-bridges labeled with rhodamine-containing RLC. (A) comparison of 1P (top) and 2P (bottom) parallel anisotropy of muscle myosin labeled with rhodamine-containing RLC. To correct for photobleaching, the anisotropy data were fitted by three-parameter exponential functions [$114.0 + 11.3e^{-0.450t}$ and $85.9 + 16.6(1 - e^{-0.007t})$ for 2P and 1P, respectively]. The fitted data was subtracted from the original data, thus, the curves are normalized to 0. The standard deviations of the signals before the flash were 1.63 and 1.36% for the 2P and 1P signals, respectively. (B) 2P parallel anisotropy of muscle exchanged with essential light chart plotted on an expanded time scale. The rising phase of the signal was fitted to a three-parameter sigmoidal (black) $r_{\parallel} = -8.97 + 5.58/(1 + \exp-[\{x - 3.32\}/0.11])$. (Reprinted with permission from Ref. 52).

probe is near (within 5 nm of) a muscle fiber, or that the probe is inserted into the muscle fiber. This is difficult to accomplish without breaking a fragile NSOM fiber tip. In addition, manufacture of NSOM probes is complex and expensive, and the method requires construction of sophisticated equipment. A simpler technique, which also uses the properties of evanescent waves but incorporates only standard microscope components, has been recently described (65). In this technique, as in the zero-mode waveguide method, the depth of focus is reduced to approximately 100 nm by the evanescent wave, but the wave is produced by the TIR from the coverslip. The *x*- and *y*-dimensions of the observational volume are limited by the confocal aperture inserted in the conjugate-image plane. The CTIR has the ability to resolve volumes on the order of a few attoliters (65). An application to fluorescence correlation spectroscopy has recently been described (66). We propose applying a modification of this method to muscle fibers. The method has never been applied to whole tissue; we provide evidence here that this can be accomplished in muscle. Table 2 summarizes the CTIR method.

The principle of the CTIR method is illustrated in Figure 4. Evanescent wave illumination is provided by the conventional TIR optics (67). The TIR effect is achieved by constraining the excitation light beam to pass only through the periphery of the objective lens. The refracted exciting beam is incident on the interface at angles greater than a critical angle, θ_c, for TIR. The evanescent field excites only those fluorophores that are very near to the interface (within ~100 nm). After excitation, emitted fluorescence is collected by the microscope objective. A confocal aperture inserted at the conjugate-image plane defines small lateral spot at the TIR surface. The aperture diameter and evanescent field depth together define the exceedingly small volume observed by the avalanche photodiode. We show in the section named "Determining the size of experimental volume," part b, that the volume is 1.5 attoliters using 3.5-μm confocal pinhole.

TIR excitation of fluorescence at a glass/buffer interface is a widely used technique in cell biology and biophysics for selectively detecting fluorophores at the interface. Many variations of the technique have been described for applications in cell biology (68–70), single molecule detection (71), and surface biophysics (72–75). TIR illumination of a glass/aqueous interface also containing an intervening thin metal layer gives rise to dramatic enhancement of transmission because of the resonant excitation of electron excitations, called surface plasmons (76). The surface plasmons propagate along the water/metal interface when the constituent materials (water and metal) have real dielectric constants with opposite signs. The evanescent electric field in TIR excitation is polarized (77). The effect of the interface on the emitted field polarization (69, 78, 79) is well understood, permitting application of this excitation-detection method to estimate fluorophore dipole orientation. Prismless TIR illumination is known to have significant background fluorescence resulting from excitation by subcritical angle light scattering (80). Alternative TIR illumination schemes using a prism to introduce excitation light to the glass/water interface at angles greater than the critical angle lowers background light levels but add the complication of a prism (69).

1. Determining the size of the experimental volume. The strategy used to estimate the volume of the voxel defined by a 3.5-μm aperture was to determine the *z*-dimension using a

Table 2. The Number of Observed Molecules Using CTIR

Method	Experimental volume (liter)	Approx. no. of cross-bridges in the volume	Degree of labeling (%)	Approx. no. of observed (fluorescent) cross-bridges
CTIR	10^{-18}	100	1	1

50-μm confocal aperture,[2] and to determine the *x*- and *y*-dimensions for a 3.5-μm aperture.

a. To determine the *z*-dimension, we experimentally determined the mean residence time, τ, of the fluorescent spheres of known size in the experimental volume. The *x*- and *y*-dimensions of the volume are known (equal to the diameter of the confocal aperture/magnification of the objective; 0.83 μm for a 50-μm aperture and a ×60 objective).[3] The spheres produce spikes in fluorescence intensity when they enter and leave the observational volume. The *z*-dimension (depth of the evanescent wave) is unknown. The relationship between the distance of translation in the *z*-direction and the residence time, τ, is a complex one.[4] The relationship depends on the known diffusion coefficient of spheres (D) and the fixed diameter of confocal aperture (d). A numerical model was constructed to estimate *z* in our experiment; from the comparison of experimental and theoretical residence times, and knowing d and D, the *z* value was determined. For the experimental determination of transit time, we used 0.1-μm diameter microspheres (Molecular Probes, Eugene, OR; carboxylate modified, λ_{ex}= 540, λ_{em}= 560 nm, 2% solids) diluted 100 times to 3.6×10^{10} spheres/ml. Figure 5 shows the intensity fluctuations caused by diffusion of the spheres through the experimental volume. Because the spikes were relatively rare (we recorded only 72 spikes during 10 secs in Fig. 5) and were separated by long periods during which the observation volume remained dark, we assumed that they were caused by a single sphere (not multiple spheres) entering and leaving the observation volume. The spheres were observed entering and leaving the volume between one and seven times. The residence (transit) time was estimated by measuring the time during which the intensity remained 87% (= $1 - 1/e^2$) of the time above the background level. The average ± SD transit time of all 72 events was 15.6 ± 7.4 msecs (n = 72; minimum = 4 msecs, maximum = 42 msecs). Theoretical simulation of the translation of spheres with a diffusion constant, D, through the detection volume, V_d, was performed by Dr. T. P. Burghardt of the Mayo Clinic (Rochester, MN). The results showed that, for a residence time of 15 ± 9 msecs, the depth of evanescent field, *z*, has to be 110 nm.

b. To estimate the *x*- and *y*-dimensions defined by a 3.5-μm aperture, we compared the amount of light collected by a 50-μm optical fiber (in which the dimensions of conjugate area are bigger than the diffraction limit) with light collected by a 3.5-μm optical fiber. The results showed that the 50-μm optical fiber collected 47 times more light than the 3.5-μm fiber. We conclude that the effective diameter of a 3.5-μm aperture in the sample plane is $0.83 / \sqrt{47} = 0.12$ μm, and that the experimental volume is approximately 1.5 attoliter.

2. Signal detection from muscle. The number of detected myosin cross-bridges is equal to C·V·A·d, where C is the concentration of myosin in muscle (120 μ*M*; Ref. 47), V is the experimental volume (~1.5 attoliter), A is Avogadro's number (6×10^{23} *M*), and d is the degree of labeling of actin with phalloidin. In muscle myofibrils, the degree of labeling can be controlled (52). Muscle was labeled with 5\'-IATR, as previously described (81). Figure 6 shows a myofibrillar A-band in a position conjugate to the confocal aperture. Extensive washing with rigor solution (50 m*M* KCl, 2 m*M* $MgCl_2$, 0.1 m*M* $CaCl_2$, 10 m*M* dithiothreitol, and 10 m*M* Tris-HCl, pH 7.6) removes free-floating and weakly attached myofibrils, leaving only the myofibrils strongly adhering to the top or bottom surfaces. The myofibrils that are attached to the top surface are too far from the evanescent wave to be fluorescent. They can be

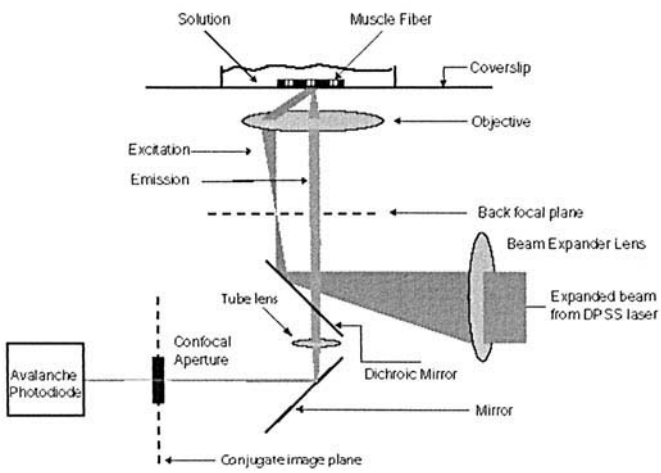

Figure 4. Prismless CTIR applied to a whole muscle fiber.

[2]The *z*-dimension is the same for 50- and 3.5-μm apertures. The advantage of using 50-μm aperture for determination of the *z*-dimension is that the *x*- and *y*-dimensions of a voxel are larger than the diffraction limit.

[3]We attempted to determine *x* and *y* experimentally by translating a sharp edge through a projection of 50-μm aperture onto the sample plane. However, the profile of an edge was dominated by the Fresnel diffraction from the edges, making the experimental determination of the aperture diameter not feasible.

[4]For a simple case of a sphere with diffusion coefficient, D, translating through a solvent, the root-mean-square translation in the *z*-direction is related to τ by Einstein's formula $z = (6D \cdot \tau)^{1/2}$.

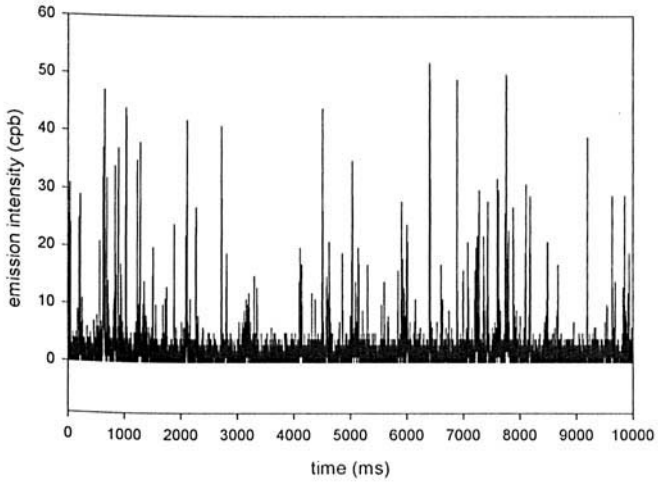

Figure 5. The fluctuations of fluorescent intensities caused by diffusion of 0.1-μm microspheres through the experimental volume defined by the 50-μm confocal aperture. Vertical scale: intensity in units of counts per bin; horizontal scale: bin width = 1 msec. The height of a peak is determined by the point of entrance of the sphere into the experimental volume, which is nonuniformly illuminated by the exponentially decaying evanescent wave.

seen out of focus with bright-field optics (Fig. 6B) but not under fluorescent light (Fig. 6A). The size of the projection of the 3.5-μm confocal aperture is shown as a white dot in the magnified image (Fig. 6C). The observational volume (Fig. 6D) is 110-nm thick and has a diameter of 120 nm, giving a volume of approximately 1.5 attoliter.

Figure 7 shows a typical signal obtained from myofibrils. Orthogonal intensities (Fig. 7A) fluctuate in time because cross-bridges change orientation. The intensities decrease in time because of photobleaching. Note that this photobleaching has a step-wise character, each step corresponding to the bleaching of one rhodamine molecule (82). The corresponding parallel polarization of fluorescence is shown in (Fig. 7B). In preliminary experiments, the power of these fluctuations in contracting muscle was always bigger than in rigor. The degree of labeling was estimated by comparing the signals of a 10 μ*M* solution of 5′-IATR with labeled myofibrils. The degree of labeling was 3%–5% and, therefore, each experimental volume contained three to five fluorescent molecules. The signal obtained from this experimental volume had a sufficient S/N ratio to allow measurements of the kinetics. The S/N ratio is

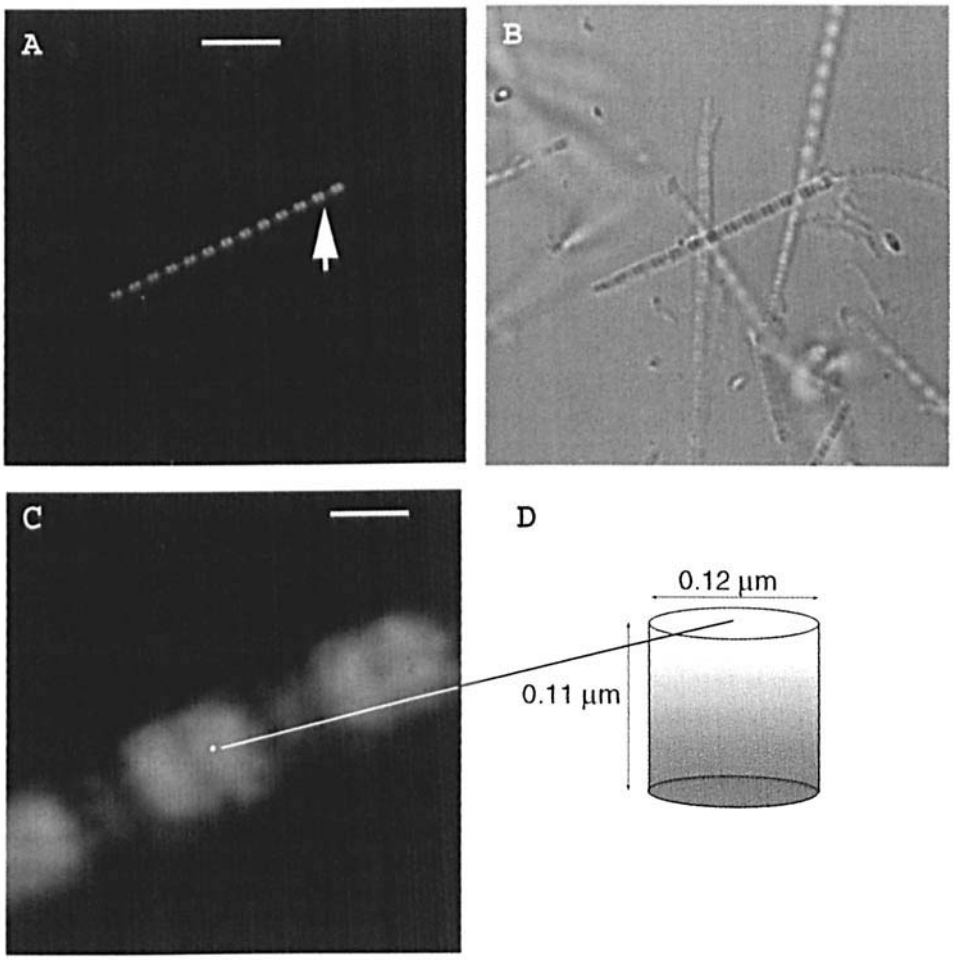

Figure 6. Image of a rigor myofibril labeled with rhodamine at cys707 of myosin. (A) Fluorescence. Bar, 10 μm. (B) Bright-field image of the area shown in (A). (C) Fluorescent image magnified ×10. Bar, 1 μm. (D) Schematic diagram of the experimental volume.

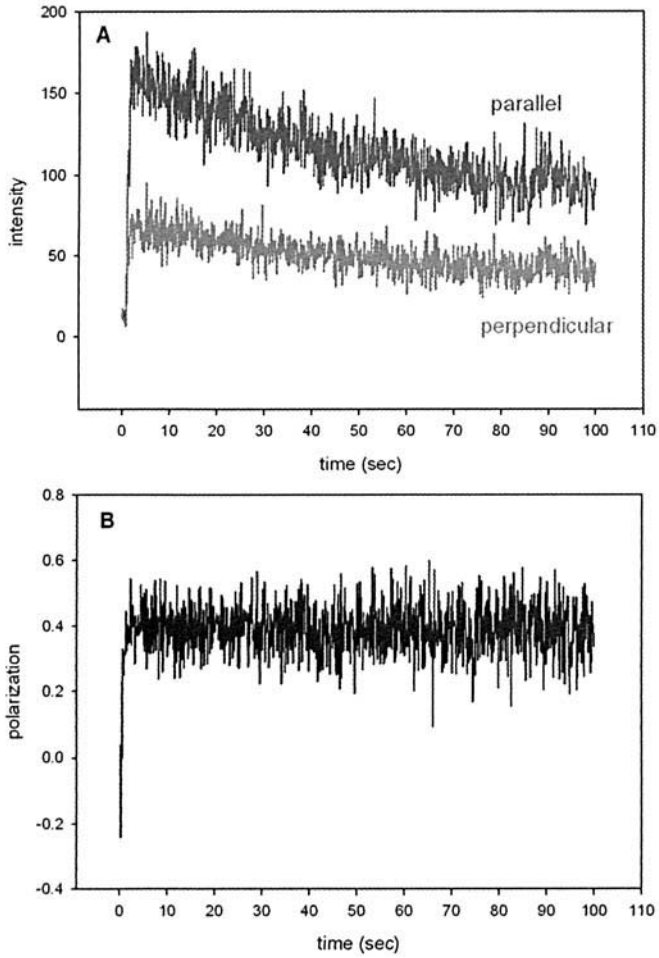

Figure 7. (A) Polarized fluorescent intensities originating from skeletal muscle myofibril in which myosin was labeled with rhodamine at cys707. (B) Corresponding parallel polarization of fluorescence, $P_{\parallel} = (I_{\parallel} - I_{\perp}) / (I_{\parallel} + I_{\perp})$.

determined by the rate of detection of fluorescent photons per molecule of the dye during one bin width, $\delta\tau$ (83). Bin width is defined as the time interval by which the data collection time is subdivided. The necessary data collection time is determined by the characteristic time for relatively slow hydrolysis, that is, approximately 0.5 sec (84). During this time, we wish to measure at least five data points, that is, giving a $\delta\tau$ of approximately 100 msecs. The preliminary data showed that we detected approximately 150 photons/molecule/bin and, assuming Poisson-distributed shot noise as the sole source of noise, the S/N ratio was approximately 12.

1. Rayment I, Rypniewski W, Schmidt-Base K, Smith R, Tomchik DR, Benning MM, Winkelman DA, Wesenberg G, Holden HM. Three-dimensional structure of myosin subfragment-1: a molecular motor. Science 261:50–58, 1993.
2. Highsmith S, Eden D. Myosin-ATP chemomechanics. Biochemistry 32:2455–2458, 1993.
3. Wakabayashi K, Tokunaga M, Kohno I, Sugimoto Y, Hamanaka T, Takezawa Y, Wakabayashi T, Amemiya Y. Small-angle synchrotron x-ray scattering reveals distinct shape changes of the myosin head during hydrolysis of ATP. Science 258(5081):443–447, 1992.
4. Uyeda TQ, Abramson PD, Spudich JA. The neck region of the myosin motor domain acts as a lever arm to generate movement. Proc Natl Acad Sci U S A 93:4459–4464, 1996.
5. Warshaw DM, Guilford WH, Freyzon Y, Krementsova E, Palmiter KA, Tyska MJ, Baker JE, Trybus KM. The light chain binding domain of expressed smooth muscle heavy meromyosin acts as a mechanical lever. J Biol Chem 275:37167–37172, 2000.
6. Dominguez R, Freyzon Y, Trybus KM, Cohen C. Crystal structure of a vertebrate smooth muscle myosin motor domain and its complex with the essential light chain: visualization of the pre-power stroke state. Cell 94:559–571, 1998.
7. Thomas DD. Spectroscopic probes of muscle cross-bridge rotation. Ann Rev Physiol 49:691–709, 1987.
8. Dos Remedios CG, Millikan RG, Morales MF. Polarization of tryptophan fluorescence from single striated muscle fibers. A molecular probe of contractile state. J Gen Physiol 59:103–120, 1972.
9. Dos Remedios CG, Yount RG, Morales MF. Individual states in the cycle of muscle contraction. Proc Natl Acad Sci U S A 69:2542–2546, 1972.
10. Nihei T, Mendelson RA, Botts J. Use of fluorescence polarization to observe changes in attitude of S1 moieties in muscle fibers. Biophys J 14:236–242, 1974.
11. Borejdo J, Putnam S. Polarization of fluorescence from single skinned glycerinated rabbit psoas fibers in rigor and relaxation. Biochem Biophys Acta 459:578–595, 1977.
12. Burghardt TP, Thompson NL. Motion of myosin cross-bridges in skeletal muscle fibers studied by time-resolved fluorescence anisotropy decay. Biochemistry 24:3731–3735, 1985.
13. Tanner JW, Thomas DD, Goldman YE. Transients in orientation of a fluorescent cross-bridge probe following photolysis of caged nucleotides in skeletal muscle fibers. J Mol Biol 223:185–203, 1992.
14. Burghardt TP, Ajtai K. Following the rotational trajectory of the principal hydrodynamic frame of a protein using multiple probes. Biochemistry 33:5376–5381, 1994.
15. Szczesna D, Graceffa P, Wang CL, Lehrer SS. Myosin S1 changes the orientation of caldesmon on actin. Biochemistry 33:6716–6720, 1994.
16. Irving M, St Claire Allen T, Sabido-David C, Craik JS, Brandmeier B, Kendrick-Jones J, Corrie JE, Trentham DR, Goldman YE. Tilting of the light-chain region of myosin during step length changes and active force generation in skeletal muscle. Nature 375:688–691, 1995.
17. Berger CL, Craik JS, Trentham DR, Corrie JE, Goldman YE. Fluorescence polarization of skeletal muscle fibers labeled with rhodamine isomers on the myosin heavy chain. Biophys J 71:3330–3343, 1996.
18. Allen TS-C, Ling N, Irving M, Goldman YE. Orientation changes in myosin regulatory light chains following photorelease of ATP in skinned muscle fibers. Biophys J 70:1847–1862, 1996.
19. Goldman YE. Wag the tail: structural dynamics of actomyosin. Cell 93: 1–4, 1998.
20. Sabido-David C, Brandmeier B, Craik JS, Corrie JE, Trentham DR, Irving M. Steady-state fluorescence polarization studies of the orientation of myosin regulatory light chains in single skeletal muscle fibers using pure isomers of iodoacetamidotetramethylrhodamine. Biophys J 74:3083–3092, 1998.
21. Corrie JE, Brandmeier BD, Ferguson RE, Trentham DR, Kendrick-Jones J, Hopkins SC, van der Heide UA, Goldman YE, Sabido-David C, Dale RE, Criddle S, Irving M. Dynamic measurement of myosin light-chain-domain tilt and twist in muscle contraction. Nature 400(6743):425–430, 1999.
22. Eisenberg E, Hill TL, Chen Y. Cross-bridge model of muscle contraction. Quantitative analysis. Biophys J 29:195–227, 1980.

23. Huxley AF. A hypothesis for the mechanism of contraction of muscle. Prog Biophys Biophys Chem 7:255–318, 1957.
24. Cooke R, Crowder MS, Thomas DD. Orientation of spin labels attached to cross-bridges in contracting muscle fibres. Nature 300(5894):776–778, 1982.
25. Berger CL, Thomas DD. Rotational dynamics of actin-bound myosin heads in active myofibril. Biochemistry 32:3812–3821, 1993.
26. Hopkins SC, Sabido-David C, Corrie JE, Irving M, Goldman YE. Fluorescence polarization transients from rhodamine isomers on the myosin regulatory light chain in skeletal muscle fibers. Biophys J. 74: 3093–3110, 1998.
27. Cooper WC, Chrin LR, Berger CL. Detection of fluorescently labeled actin-bound cross-bridges in actively contracting myofibrils. Biophys J 78:1449–1457, 2000.
28. Funatsu T, Harada Y, Tokunaga M, Saito K, Yanagida T. Imaging of single fluorescent molecules and individual ATP turnovers by single myosin molecules in aqueous solution. Nature 374:555–559, 1995.
29. Ishijima A, Kojima H, Funatsu T, Tokunaga M, Higuchi H, Tanaka H, Yanagida T. Simultaneous observation of individual ATPase and mechanical events by a single myosin molecule during interaction with actin. Cell 92:161–171, 1998.
30. Warshaw DM, Hayes E, Gaffney D, Lauzon AM, Wu J, Kennedy G, Trybus K, Lowey S, Berger C. Myosin conformational states determined by single fluorophore polarization. Proc Natl Acad Sci U S A 95:8034–8039, 1998.
31. Forkey JN, Quinlan ME, Shaw MA, Corrie JE, Goldman YE. Three-dimensional structural dynamics of myosin V by single-molecule fluorescence polarization. Nature 422(6930):399–404, 2003.
32. Minton AP. Molecular crowding: analysis of effects of high concentrations of inert cosolutes on biochemical equilibria and rates in terms of volume exclusion. Methods Enzymol 295:127–149, 1998.
33. Arakawa T, Timasheff SN. Theory of protein solubility. Methods Enzymol 114:49–77, 1985.
34. Bhat R, Timasheff SN. Steric exclusion is the principal source of the preferential hydration of proteins in the presence of polyethylene glycols. Protein Sci 1:1133–1143, 1992.
35. Minton AP, Wilf J. Effect of macromolecular crowding upon the structure and function of an enzyme: glyceraldehyde-3-phosphate dehydrogenase. Biochemistry 20:4821–4826, 1981.
36. Minton AP. The influence of macromolecular crowding and macromolecular confinement on biochemical reactions in physiological media. J Biol Chem 276:10577–10580, 2001.
37. Arakawa T, Timasheff SN. Mechanism of poly(ethylene glycol) interaction with proteins. Biochemistry 24:6756–6762, 1985.
38. Highsmith S, Duignan K, Franks-Skiba K, Polosukhina K, Cooke R. Reversible inactivation of myosin subfragment 1 activity by mechanical immobilization. Biophys J 74:1465–1472, 1998.
39. Peyser YM, Shaya S, Ajtai K, Burghardt TP, Muhlrad A. Cosolvent induced aggregation inhibits myosin ATPase activity by stabilizing the predominant transition intermediate. Biochemistry 42:12699–12675, 2003.
40. Andreev OA, Borejdo J. Myosin head can bind two actin monomers. Biochem Biophys Res Comm 177:350–356, 1991.
41. Andreev OA, Andreeva AL, Markin VS, Borejdo J. Two different rigor complexes of myosin subfragment-1 and actin. Biochemistry 32: 12046–12035, 1993.
42. Itakura S, Yamakawa H, Toyoshima YY, Ishijima A, Kojima T, Harada Y, Yanagida T, Wakabayashi T, Sutoh K. Force-generating domain of myosin motor. Biochem Biophys Res Commun 196:1504–1510, 1993.
43. Tokunaga M, Iwane A, Kitamura K, Yanagida T. S1 attachment to a glass surface through a flexible random chain can move actin as fast as intact myosin. Biophys J 76:A36, 1999.
44. Tanaka H, Iwane Hikikossi A, Okamura T, Morimoto S, Kusumoto T, Ishijima A, Yanagida T. Role of myosin neck region in generation of movement. Biophys J 78:234A, 2000.
45. Yanagida T. Loose coupling between chemical and mechanical reactions in actomyosin energy transduction. Adv Biophys 26:75–95, 1990.
46. Brust-Mascher I, LaConte LE, Baker JE, Thomas DD. Myosin light-chain domain rotates upon muscle activation but not ATP hydrolysis. Biochemistry 38:12607–12613, 1999.
47. Bagshaw CR. Muscle Contraction. London: Chapman & Hall, 1982.
48. Eigen M, Rigler R. Sorting single molecules: application to diagnostics and evolutionary biotechnology. Proc Natl Acad Sci U S A 91:5740–5747, 1994.
49. Borejdo J, Ushakov DS, Akopova I. The regulatory and essential light chains of myosin rotate equally during contraction of skeletal muscle. Biophys J 82:3150–3159, 2002.
50. Borejdo J, Akopova I. Orientational changes of cross-bridges during single turnover of ATP. Biophys J 84:2450–2459, 2003.
51. Borejdo J, Shepard A, Dumka D, Akopova I. Anisotropy of myosin and actin during contraction of skeletal muscle. In: Pandalai SG, Eds. Recent Research Developments in Biophysics. Kerala, India: Trans-World Research Network, Vol2:pp191–207, 2003.
52. Borejdo J, Shepard AA, Akopova I, Grudzinski W, Malicka J. Rotation of the lever-arm of myosin in contracting skeletal muscle fiber measured by two-photon anisotropy. Biophys J 87:3912–3921, 2004.
53. Pawley JB. Handbook of Biological Confocal Microscopy (2nd ed.). New York and London: Plenum Press, 1995.
54. Shepard AA, Dumka D, Akopova I, Talent J, Borejdo J. Simultaneous measurement of rotations of myosin, actin and ADP in contracting skeletal muscle fiber. J Muscl Res Cell Mot 25:549–557, 2004.
55. Borejdo J, Shepard A, Dumka D, Akopova I, Talent J, Malka A, Burghardt TP. Changes in orientation of actin during contraction of muscle. Biophys J 86:2308–2317, 2004.
56. Borejdo J, Ushakov DS, Akopova I. The essential light chains 1 and 3 rotate differently during muscle contraction. Biophys J 82:362a, 2002.
57. Hubley MJ, Locke BR, Moerland TS. The effects of temperature, pH, and magnesium on the diffusion coefficient of ATP in solutions of physiological ionic strength. Biochim Biophys Acta 1291:115–121, 1996.
58. Borejdo J. Tension fluctuations in contracting myofibrils and their interpretation. Biophys J 29:49–63, 1980.
59. Borejdo J. Application of fluctuation spectroscopy to muscle contractility. Curr Top Bioenergetics 10:1–50, 1980.
60. Hill TL, Eisenberg E, Chen YD, Podolsky RJ. Some self-consistent two-state sliding filament models of muscle contraction. Biophys J 15: 335–372, 1975.
61. Levene MJ, Korlach J, Turner SW, Foquet M, Craighead HG, Webb WW. Zero-mode waveguides for single-molecule analysis at high concentrations. Science 299(5607):682–686, 2003.
62. Hecht B, SB, Wild UP, Deckert V, Zenobi R, Martin OJ. Scaning near-field optical microscopy with aperture probes: fundamentals and applications. J Chem Phys 112:7761–7774, 2000.
63. Dunn RC. Near-field scanning optical microscopy. Chem Rev 99: 2891–2927, 1999.
64. Betzig E, Chichester RJ. Single molecules observed by near field scanning optical microscopy. Science 262:1422–1425, 1993.
65. Ruckstuhl T, Seeger S. Attoliter detection volumes by confocal total-internal-reflection fluorescence microscopy. Opt Lett 29:569–571, 2004.
66. Hassler K, Anhut T, Rigler R, Gosch M, Lasser T. High count rates with total internal reflection fluorescence correlation spectroscopy. Biophys J 88:L01–L03, 2005 (Epub Nov 05, 2004).
67. Axelrod D. Total internal reflection fluorescence microscopy. Methods Cell Biol 30:245–270, 1989.
68. Axelrod D. Cell-substrate contacts illuminated by total internal reflection fluorescence. J Cell Biol 89:141–145, 1981.

69. Axelrod D. Total internal reflection fluorescence microscopy in cell biology. Traffic 2:764–774, 2001.
70. Johns LM, Levitan ES, Shelden EA, Holz RW, Axelrod D. Restriction of secretory granule motion near the plasma membrane of chromaffin cells. J Cell Biol 153:177–190, 2001.
71. Sako Y, Minoghchi S, Yanagida T. Single-molecule imaging of EGFR signalling on the surface of living cells. Nat Cell Biol 2:168–172, 2000.
72. Thompson NL, Burghardt TP, Axelrod D. Measuring surface dynamics of biomolecules by total internal reflection fluorescence with photobleaching recovery or correlation spectroscopy. Biophys J 33:435–454, 1981.
73. Burghardt TP, Axelrod D. Total internal reflection/fluorescence photobleaching recovery study of serum albumin adsorption dynamics. Biophys J 33:455–467, 1981.
74. Axelrod D, Hellen EH. Emission of fluorescence at an interface. Methods Cell Biol 30:399–416, 1989.
75. Sund SE, Axelrod D. Actin dynamics at the living cell submembrane imaged by total internal reflection fluorescence photobleaching. Biophys J 79:1655–1669, 2000.
76. Ford GW, Weber WH. Electromagnetic interactions of molecules with metal surfaces. Phys Rep 113:195–287, 1984.
77. Burghardt TP, Thompson NL. Evanescent intensity of a focused gaussian light beam undergoing total internal reflection in a prism. Optical Engineering 23:62–67, 1984.
78. Hellen EH, Axelrod D. Fluorescence emission at dielectric and metal-film interfaces. J Opt Soc Am B 4:337–350, 1987.
79. Thompson NL, Burghardt TP. Total-internal reflection fluorescence: measurement of spatial and orientational distributions of fluorophores near planar dielectric interfaces. Biophys Chem 25:91–97, 1986.
80. Mattheyses A, Axelrod D. Direct measurement of evanescent field profile and depth in TIRF microscopy. Biophys J 86:320a, 2004.
81. Borejdo J, Assulin O, Ando T, Putnam S. Cross-bridge orientation in skeletal muscle measured by linear dichroism of an extrinsic chromophore. J Mol Biol 158:391–414, 1982.
82. Eggeling C, Widengren J, Rigler R, Seidel CAM. Photobleaching of fluorescent dyes under conditions used for single-molecule detection: evidence of two-step photolysis. Anal Chem 70:2651–2659, 1998.
83. Magde D, Elson EL, Webb WW. Fluorescence correlation spectroscopy. II. An experimental realization. Biopolymers 13:29–61, 1974.
84. Potma EJ, van Graas IA, Stienen GJ. Effects of pH on myofibrillar ATPase activity in fast and slow skeletal muscle fibers of the rabbit. Biophys J 67:2404–2410, 1994.